JOURNAL OF MATERIALS SCIENCE: MATERIALS IN MEDICINE 12 (2001) 225–231

Titanium powder sintering for preparation of a porous functionally graded material destined for orthopaedic implants

M. THIEME, K.-P. WIETERS, F. BERGNER, D. SCHARNWEBER, H. WORCH, J. NDOP*, T. J. KIM*, W. GRILL*
*Dresden University of Technology, Institute of Materials Science, D–01062 Dresden, Germany and *University of Leipzig, Institute for Experimental Physics II, Linnéstr. 5, D-04103 Leipzig, Germany*
E-mail: mithi@rcs.urz.tu-dresden.de

This work focuses on basic research into a P/M processed, porous-surfaced and functionally graded material (FGM) destined for a permanent skeletal replacement implant with improved structural compatibility. Based on a perpendicular gradient in porosity the Young's modulus of the material is adapted to the elastic properties of bone in order to prevent stress shielding effects and to provide better long-term performance of the implant-bone system. Using coarse Ti particle fractions the sintering process was accelerated by silicon-assisted liquid-phase sintering (LPS) resulting in a substantial improvement of the neck geometry. A novel evaluation for the strength of the sinter contacts was proposed. The Young's modulus of uniform non-graded stacks ranged from 5 to 80 GPa as determined by ultrasound velocity measurements. Thus, the typical range for cortical bone (10–29 GPa) was covered. The magnitude of the Poisson's ratio proved to be distinctly dependent on the porosity. Specimens with porosity gradients were successfully fabricated and characterized using quantitative description of the microstructural geometry and acoustic microscopy.

1. Introduction

The replacement of tissues and complete organs damaged by disease or trauma is a challenge for materials science. In the case of the skeletal system, biomaterials must possess adequate mechanical, morphological and physico-chemical properties to achieve a high degree of biocompatibility and biofunctionality. For these purposes, metals are the most important materials class because of their load-bearing ability [1]. However, the stiffness of the implantable metallic devices is, preferentially for total hip arthroplasty, generally not well adapted. This situation leads to stress shielding from the residual bone, which may result in detrimental resorptive bone remodeling [2] so that the long-term performance as an essential prerequisite for a permanent replacement may be affected.

As the stiffness of a device is determined by the Young's moduli of the material used (besides its moment of inertia of an area), a critical consideration of this quantity is justified. In the case of metallic implant materials its magnitude surpasses that of cortical bone by far (Table I) and points to a drastic mismatch.

In order to bridge this mismatch, the idea was born, to prepare a sintered porous coating on a conventional solid implant stem with a gradient of the porosity $P(x)$ perpendicular to the long axis. This geometry is accompanied with a gradient of the Young's modulus $E(P, x)$, which has the opposite direction to that of the porosity and should change from the value of the compact material E_0 down to the level of cortical bone E_b. In this way, a functionally graded material (FGM) would be generated, which is a basis to approach the isoelastic-implant concept.

Clearly, the magnitude of the maximum porosity of the gradient must be adjusted in an appropriate manner, where also the strength behavior of the sintered stacks must be taken into consideration. Additionally, there are limitations due to the ingrowth of the bone tissue and its vascularization. According to earlier findings based on animal implantation studies with porous model specimens [9–11] optimal ranges exist in both the pore width and porosity. They were given to be 100–400 μm and 0.2–0.5, respectively.

Surveying the corresponding literature there are a large number of investigations that have also studied porous-surfaced, but non-graded systems. A detailed overview was recently given by Pilliar [12]. In most cases the investigations aimed at achieving a better mechanical interlock between implant and bone. Two recent studies are explicitly mentioned, where elastic adaptation was attempted. Here, porous coatings were additionally combined with changes in the composition or type of the materials: *i* – Ti30Ta with $E_0 = 81-64$ GPa (depending on the actual microstructural state) and

TABLE I Comparison of literature data for the Young's moduli of different metallic implant materials and human cortical bone (in GPa)

Ti, annealed	Ti6Al4V, annealed	Co29Cr5Mo, cast	Stainless steel ASTM 316L	Cortical bone
112 [3]	115 [3]	200 [4]	210 [4]	12–23 (tensile) [5], 14–29 (tensile) [6], 10–13/19–21 (transvers./longit. directions, ultrasound) [7], 15–17/19–26 (transvers./longit. directions, nanoindent) [8]

$E_{p=0.3} = 25$ GPa [13]; *ii*–nanoporous glassy carbon with 17–40 GPa [14].

The present contribution refers to basic research within the development of such an FGM type. It focuses on *i* – the preparation of beam-like model specimens in order to study how the experimental variables influence the general sintering behavior, the porosity, the strength of the sinter contacts and the elastic properties, *ii* – the feasibility of the sinter-technological preparation of porosity and modulus gradients and *iii* – the selection and adaptation of appropriate testing methods.

The experimental work was confined to titanium as to one of the most important biometals, regardless of unfavorable grain coarsening due to high-temperature annealing.

Concerning the choice of the powder size, relatively coarse particle fractions were selected in view of the necessary pore width. However, this is accompanied with a disadvantageous decrease of the sinter rate and the strength so that appropriate countermeasures had to be examined.

2. Experimental

2.1. Preparation conditions

Spherical cp titanium particles generated by the plasma rotating electrode process (PREP) [15] were used involving five fractions within the diameter range of $D = 180$–$1000\,\mu m$. One of these fractions consisted of agglomerated particles. Sintering was done under different regimes ($T_s = 1150$–$1500\,^{\circ}C$, $t_s = 1$–$6\,h$, one-step or two-step process) using a high-vacuum oven (*ca.* 2 mPa). Ceramic molds were fabricated for producing beam-like specimens ($4 \times 6 \times 29\,mm^3$). The two-step process (1150 °C, 1 h; non-compressed stacks in a Si_3N_4 mold) + (1470 °C, 1 h; specimens resting on a W or ZrO_2 support) was designated as the standard procedure (std). Additionally, flat-cylindrical stacks with an outer Ti tube segment (height 2.5 mm, ∅10.9 mm) or specimens with compact Ti supports were sintered. As an additive, fine-grained silicon powder (< 32 µm) was added by (A) infiltration of ethanolic suspensions after pre-sintering, (B) mixing of powder suspensions with ethanol-dissolved poly-(vinylpyrrolidon) as binder (B1) or with toluene-dissolved polysilane copolymer (B2), and (C) milling using a planete ball mill (maximum 6 h).

Graded stacks were formed by combination of powder layers distinguished by particle size and Si additive concentration.

For comparison, bone specimens of beam-like shape were cut off a human tibia (female, age 91 yrs) and stored in isotonic NaCl solution.

2.2. Characterization

Light microscopy was extensively used after cross-sectioning and polishing the specimens along with scanning electron microscopy (SEM) and electron probe microanalysis (EPMA).

The (volume fraction) porosity P of the sintered specimens was calculated from mass and geometric dimensions (P_{geo}) as well as from the immersion-penetration method utilizing the Archimedean principle (P_{ipm}). The latter comprised a set of four weighings (in air, under immersion in paraffin oil, in air and in water after oil-soaking) additionally allowing the discrimination of the open and closed porosities. The bending strength σ_b was determined through the three-point bending test (1 mm min^{-1}) according to Equation 1

$$\sigma_b = 1.5 \cdot F_{max} \cdot d/(w \cdot h^2) \quad (1)$$

where F_{max} = maximum force at fracture, d = distance of the supports, w = width and h = height of the specimens.

The determination of the Young's modulus E was based on longitudinal-wave ultrasound measurements using transmission geometry (transducers of 2.2 MHz) under immersion in water, where the sound velocity c_l of the specimens was determined from the time difference Δt taking the first received points of the output signals without and with insertion of the stacks

$$c_l = (1/c_w - \Delta t/w)^{-1},$$
$$E = c_1^2 \cdot (1 - P) \cdot \rho_o \cdot (1 + \nu) \cdot (1 - 2\nu)/(1 - \nu) \quad (2)$$

(c_w = sound velocity in water, ρ_o = density of the compact material (4.51 g/cm^3), ν = Poisson's ratio). Additionally, longitudinal and transverse velocity measurements [16] were performed under solid acoustic coupling, which allowed determination of the Poisson's ratio including its porosity dependence

$$\nu = [0.5 - (c_t/c_l)^2]/[1 - (c_t/c_l)^2] \quad (3)$$

This procedure required a more expensive preparation of the specimens. They were sliced of selected sintered stacks, ground and polished, finally having a thickness of about 3 mm with two flat and parallel surfaces.

In the case of graded specimens, the local porosity was estimated by quantitative description of the microstructural geometry, whereas the local elastic properties were derived from phase-sensitive scanning acoustic microscopy (PSAM) [17].

3. Results and discussion

3.1. Sintering of pure Ti powders

The metallographic examination of the cross-sections of non-graded specimens showed interpenetrating networks of the sintered solid and of the pore channels. Relatively sharp neck profiles corresponding to low dihedral angles were observed, preferentially with coarse powder fractions. For these cases, the growth of the necks appeared to stagnate at about 100 µm in spite of intensifying the sinter conditions.

The bending strength covered a wide range with a pronounced inverse dependence on the particle size. This may be favorably displayed in the diagram σ_b versus $1/D^2$ (Fig. 1). The two-step std procedure proved to be clearly superior to one-step sintering under varied T_s and t_s conditions.

The porosity was in the range of 0.35–0.6, the highest values occurring with agglomerated powder. Closed porosity could be neglected in most cases.

The longitudinal sound velocities showed, as expected, an inverse dependence on porosity. The Young's modulus amounted to 5–35 GPa (std), where preliminarily $\nu = \nu_0 = 0.32$ was taken for the calculation (Equation 2). The issue of the magnitude of the Poisson's ratio will be discussed below in greater detail.

The results using pure Ti powders revealed that deficits occurred mainly in the field of the microstructural geometry. As a consequence, efforts were made to accelerate the sintering process.

3.2. Evaluation of the bending strength

It was felt that the relevance of the quantity ''bending strength'' was inadequate in view of the mechanical loading under service conditions. Whereas in the latter case the (shear) strength of the *single sinter contact* is of crucial importance, σ_b refers to the *ensemble* of the sinter contacts, where the strength is determined by the minimum solid area normal to the stress [18]. Thus, it is possible to characterize the properties of the single contacts in a more proper way, if the number of the sinter contacts n_{con} is taken into consideration. Obviously, for a given specimen geometry n_{con} is a function of the particle size and the coordination number. Therefore, the relation holds

$$n_{con} \propto (1/D^2) \cdot (1 - P)^x \tag{4}$$

where x equals to 1, according to [19].

Based on these considerations, the modified bending strength σ^* was defined as follows

$$\sigma^* = \sigma_b \cdot D^2/(1 - P) \tag{5}$$

It has the dimension of a force with the unit 1 MPa mm^2 = 1 N. However, this quantity should not be identified with the force necessary for breaking off one particle or so, because the sinter neck area was not explicitely taken into consideration. Comparing σ^* data for sintered stacks composed of different particle sizes, it is seen that the quality of the single contacts using coarse particles is not worse than using fine-grained particles. Table II displays corresponding data sets obtained for std procedure-sintered specimens (average diameter $\bar{D} = 0.22 \rightarrow 0.85$ mm). The original bending strength data form a decreasing rank, which suggests that the quality of the sintered stacks would decrease with increasingly coarse particles. Contrarily, the adverse rank of the σ^* values expresses that this assumption is not justified.

TABLE II Comparison of strength data determined for sintered beam-like stacks formed of different Ti particle fractions using standard procedure

$D_{min,max}/mm$	0.18/0.25	0.25/0.40	0.40/0.50	0.50/0.70	0.70/1.00
σ_b/MPa	184	97	48	40	26
σ^*/N	13	17	21	25	37

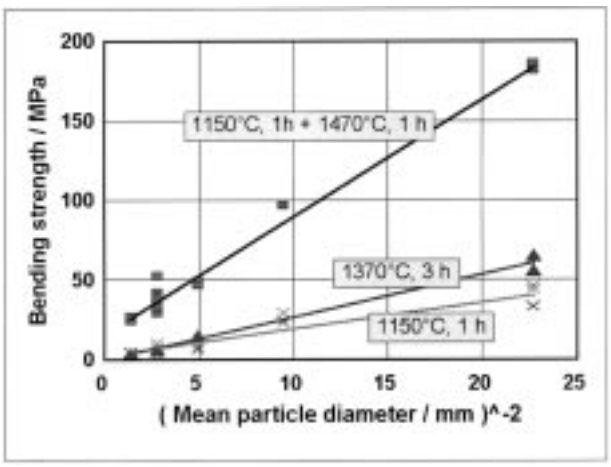

Figure 1 Bending strength of sintered specimens (pure Ti, selected sinter conditions) versus reciprocal square of the mean particle diameter of the fractions used; lines according to linear regression.

3.3. Sintering of Ti with silicon additions

Silicon has been chosen as an additive for the sintering of coarse Ti particles based on the eutectic at 1330 °C, 13.5 at % ≙ 8.4 wt % Si [20], which could be utilized for liquid-phase sintering LPS. The phase diagram also makes clear that cooling down will be accompanied by a number of transformations which eventually lead to the α Ti matrix with < 0.5 at % Si for < 865 °C and the silicide precipitates Ti_5Si_3 and Ti_3Si. The necessary additive amount was estimated on the assumption that a circumferential layer of 10 µm thickness should be liquified, thus promoting the formation of the sinter necks between neighboring particles. E.g., the use of the fraction with $\bar{D} = 0.6$ mm would require a Si concentration of only 0.78 wt %.

Practically, the particles had to be provided with the calculated Si amount to achieve a relatively stable and uniform coverage. Different variants were examined, as is documented in the experimental section. Following the procedures B or C, LPS was induced for Si concentrations of 1.5 wt % and more in the case of the 500/700 µm fraction. These conditions succeeded in producing a satisfactory sinter neck geometry characterized by

Figure 2 Sinter neck geometry of a non-graded specimen achieved by the addition of 1.5 wt % Si to spherical Ti particles (500/700 µm; milled; 1510 °C, 1 h; cross-sectioned; light-microscopy).

increased neck radii and dihedral angles (Fig. 2). Typical neck diameters were in the range of 300–400 µm, i.e. more than $0.4 \times D$, which was considered as a minimum limit for a suitable structure [12]. On the other hand, infiltration of Si into pre-sintered specimens (procedure A) gave an inhomogeneous distribution within the specimens causing undesirable melting effects in the outer zone.

Tracing the fate of the added silicon, EPMA showed that milling, which gives the most uniform and stable Si coating, does not lead to superficial alloying per se. Pre-sintering at 1150 °C generates a thin alloyed layer (Fig. 3), whereas the final sintering step results in a uniform distribution of the Si precipitated as fine-dispersed silicides within the beads.

It should be noted for completeness that the attempt failed to incorporate silicon by the application of the relatively Si-rich, liquid copolymer polydimethylsilane-methylphenylsilane. Summarizing, the chosen approach utilizing elemental Si as a sinter additive proved to be a very effective means for inducing LPS and, hence, progressing the sintering process of Ti. Localized LPS is also effective in the case of Co-Cr-Mo alloys, the alternative material type for total hip arthroplasty, at temperatures of more than about 1250 °C [12]. However,

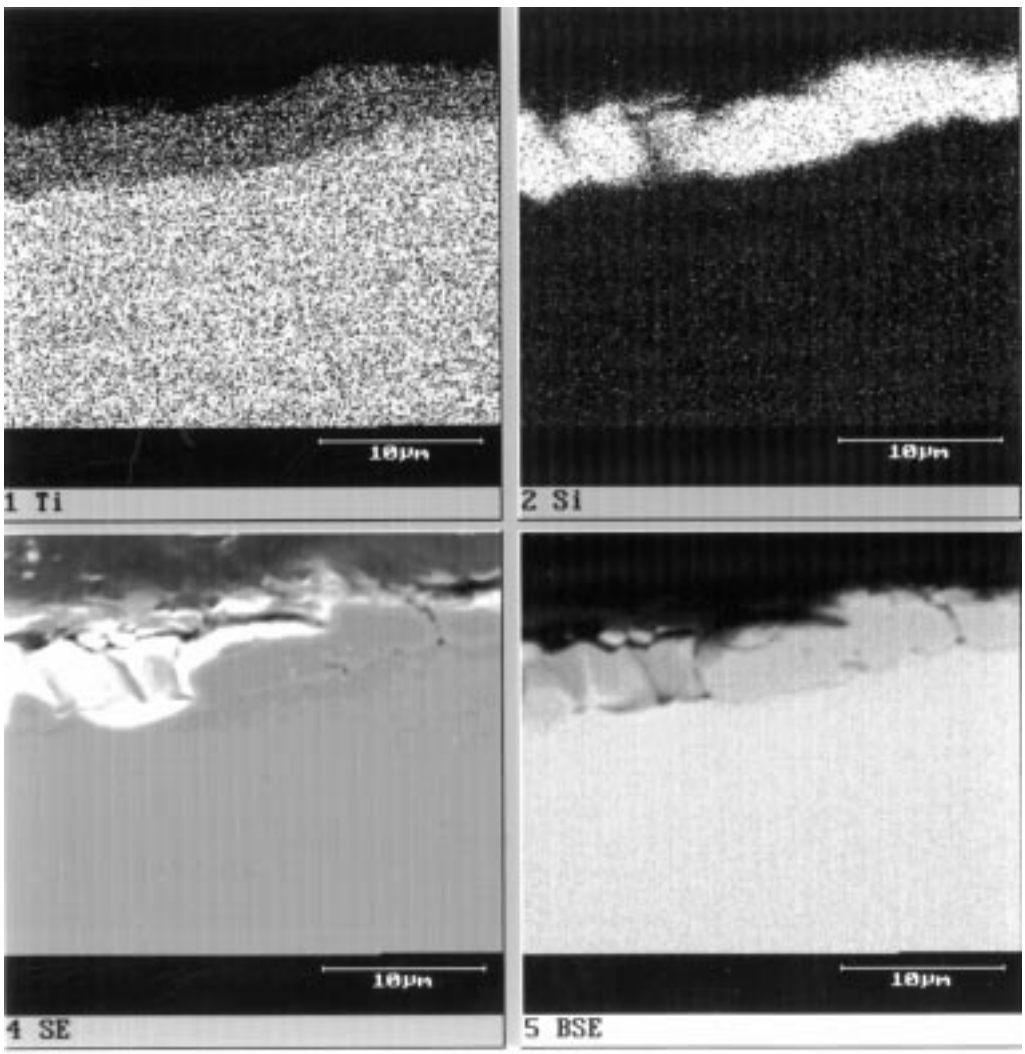

Figure 3 EPMA elemental analyses (*l.*-Ti, *r.*-Si) and SEM images on a pre-sintered specimen (Ti 500/700 µm + 2.4 wt % Si; milled; 1150 °C, 1 h; cross-sectioned).

here it is accompanied with the presence of inherent phases.

The use of Si may provoke the concern that it might affect the high biocompatibility level of Ti. However, this concern can be rejected referring to findings of earlier works: *i* – Si represents the major component of bioinert ceramic implant materials of the type Al_2O_3-SiO_2-TiO_2 [21]. *ii* – Ti_5Si_3 coverages on Ti6Al4V were shown to promote the attachment of bone tissue [22]. It is additionally mentioned that the formation of bioactive apatite from simulated body fluid was favored by SiO_2 and silicate ions generated by silica [23].

The bending strength of LPS-modified specimens produced from coarse particles was not thoroughly changed. The procedure B1 gave a vague increase, whereas milling (C) led to a slight decrease with increasing Si concentration. The latter finding may be explained by the less dense package of the beads, which is caused by the increased roughness of the coated particles and, hence, by worsened flow properties. The bending strength of cortical bone was about 175 MPa.

The porosity dependence of the bending strength of the sintered specimens is documented in Fig. 4, where all the results were collected including those using bi- and trimodal mixtures of Ti particles. The behavior may be roughly described by Equation 6, which was found to be valid for porous glasses, ceramics and metals [24]

$$\sigma = \sigma_o \cdot (1 - P)^K \tag{6}$$

where $K =$ stress concentration factor and $\sigma_o =$ bending strength of the compact material. K was shown to vary in a wide range in dependence on the aspect ratio and the orientation of the pores. However, in the present case the fitted values ($\sigma_o = 1800\ MPa, K = 5.5$) are not meaningful, because compact Ti has undergone plastic deformation instead of fracture, and the restriction to isolated spheroidal pores does not apply at all.

The Young's modulus was calculated according to Equation 2 taking preliminarily $\nu = \nu_o = 0.32$. Fig. 5 displays the data again as a whole in order to illustrate the porosity dependence of the modulus. Comparing the

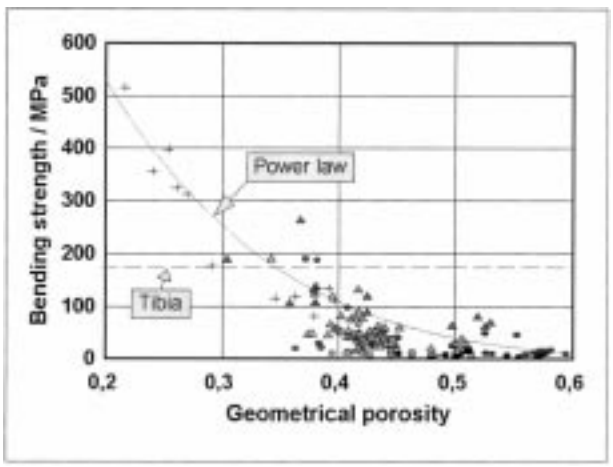

Figure 4 Bending strength versus porosity for sintered specimens using cp Ti fractions (circles), Ti + Si (triangles) and Ti particle mixtures (crosses); results for tibia for comparison; modeling: power law according to Equation 6 [24] (see text).

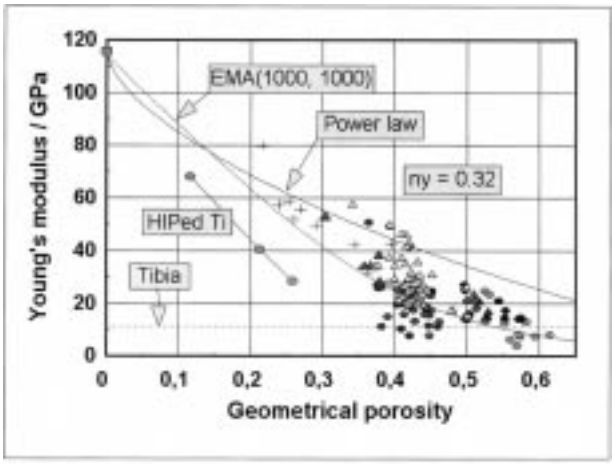

Figure 5 Young's modulus versus porosity for sintered specimens using cp Ti fractions (circles), Ti + Si (triangles) and Ti particle mixtures (crosses) as calculated using $\nu = 0.32$; additional data for compact Ti (square), HIPed Ti [27] (ν acc. to Equation (9)) and tibia ($\nu = 0.33$ averaged from [7]); modeling: power law according to $E = E_o(1 - P^{2/3})^{1.21}$ [25], effective-medium approach [26] (see text).

results for the same powder sizes and sintering conditions the addition of Si caused a shift to higher modulus values along with decreased porosities. Altogether, a range of $E = 5-60$ GPa is obtained. The upper limit is shifted to about 80 GPa, if specimens with lower porosities are included, which were made from bi- or trimodal mixtures of Ti bead fractions. Additionally, the diagram displays data for compact Ti (115 GPa) and for hot-isostatically pressed Ti based on ultrasound measurements of Ledbetter *et al*. [28]. The line designated by ''tibia'' refers to the data range of 11–13 GPa as determined in this work for human tibia material in the transverse direction, which agrees with the corresponding literature data (Table I). It can be seen that the lower end of the modulus range for sintered Ti overlaps well with that for cortical bone, i.e. the target of the elastic adaptation may be achieved. Thus, the prerequisite is given to construct FGM model specimens with gradually changing profiles of porosity and, hence, of Young's modulus.

Concerning the quantitative description of the porosity dependence of the modulus data, a power law similar to Equation 6 was applied [25] as well as the effective-medium approach EMA [26] (Fig. 5). The latter appears to give a slightly better fit. Thereby a mixture of rod-like solid particles and pores of the same shape was adopted, where an aspect ratio c/a as high as 1000 was chosen in view of the specific microstructure of the sintered specimens. The same principal agreement was obtained for c/a = 100.

Following the chosen route according to Equation 2 for the determination of E, a completely correct calculation requires the knowledge of the appertaining Poisson's ratio. To solve this problem, a number of sintered specimens covering a wide porosity range was selected, prepared and measured using longitudinal and transverse ultrasound in the manner described in section 2.2. These experiments indicated that there is a significant porosity dependence of the Poisson's ratio $\nu(P)$. However, this issue shall be discussed in a separate paper referring to different theoretical approaches.

3.4. Sintered specimens with porosity gradients

Based on the results for porosity and modulus obtained for the variety of specimen types, a number of different graded structures were designed, fabricated and examined. The cross-section of one of them (type #I) is shown in Fig. 6a.

Table III provides data determined by quantitative microstructural analysis for the two structures #I and #II with three sublayers each, which are distinguished only by the fraction used for the uppermost sublayer. The porosities and the mean chord lengths as a measure for the pore size were found to change monotonically from sublayer to sublayer as had been intended (significance tested for $\alpha = 0.05$).

The local elastic properties of graded porous-sintered specimens were characterized by PSAM studies. The longitudinal velocity was derived from the phase shift of the response signal transmitted through the sliced specimen. Fig. 6b shows the results for two scans along the gradient, whose cross-section is seen in Fig. 6a. It is demonstrated that the profile of the velocity and, hence, of the Young's modulus is inversely connected with the change of the porosity. If the c_i data determined for the base and top sublayers of the gradient #1 are combined with Poisson's ratios appertaining to the measured porosities (Table III), then the following data triples are obtained.

$$- c_{l,loc} = 3.2\,\mathrm{km\,s^{-1}}; P_{loc} = 0.22; \nu_{loc} \approx 0.3$$
for the base sublayer;

$$- c_{l,loc} = 2.2\,\mathrm{km\,s^{-1}}; P_{loc} = 0.45; \nu_{loc} \approx 0.4$$
for the top sublayer.

From this, $E_{loc,base} = 26\,\mathrm{GPa}$ and $E_{loc,top} = 5.6\,\mathrm{GPa}$ are calculated according to Equation 2. These results make clear that there is a gradient in the elastic behavior indeed. However, uncertainties in the absolute magnitudes of the moduli may occur. These uncertainties are caused by deviations of the local-quantity scales from those established by the measurements of the bulk porosities and the bulk velocities, respectively, which were the basis of the actual relationship between porosity and the Poisson's ratio.

TABLE III Porosities P_{loc} and mean chord lengths L according to the quantitative description of the microstructural geometry as measured on two three-sublayered structures (Ti rings Ø12.7/10.9 × 6 mm as outer cladding; 1470 °C, 3 h). Average of 12 data sets (standard deviations in brackets) were calculated based on three section levels, where four rectangular measuring fields (3.26 mm²) were positioned side by side for each sublayer

Sublayer	#I, base	#I, middle	#I, top	#II, base	#II, middle	#II, top
Powder	125/180 µm	250/400 µm + 1.7% Si	400/500 µm (aggl.) + 1.6% Si	ditto	ditto	500/700 µm + 2.4% Si
P_{loc}	0.222 (0.031)	0.299 (0.026)	0.448 (0.059)	0.226 (0.028)	0.302 (0.056)	0.376 (0.078)
L/µm	48 (6)	106 (9)	200 (33)	48 (5)	114 (13)	311 (58)

4. Conclusions

It can be concluded that the conception of adapting the elastic properties of metallic implant materials to that of bone may be successfully put into practice with a sintered porous surface having a porosity gradient perpendicular to the surface.

In the case of coarse-beaded porous-sintered titanium the application of fine-grained Si as a secondary powder component proved to be a crucial prerequisite for generating a satisfactory microstructure based on liquid-phase sintering. The notch sensitivity will have been diminished in this way, but local stress concentration cannot be eliminated under load. Hence, appropriate fatigue testing must be accomplished as has been done in the case of conventionally sintered and other types of porous coatings on Ti and Ti6AlV4 (e.g. [28]).

The proposal concerning an additional evaluation of the strength of sintered structures may be a panel for further discussion. The issue concerning the dependence of the Poisson's ratio on the pore properties will be separately published.

Likewise, the results obtained by cell culture testing of sintered specimens provided with different porosity gradients and collagen or electrochemically deposited hydroxyapatite coverages will be described elsewhere.

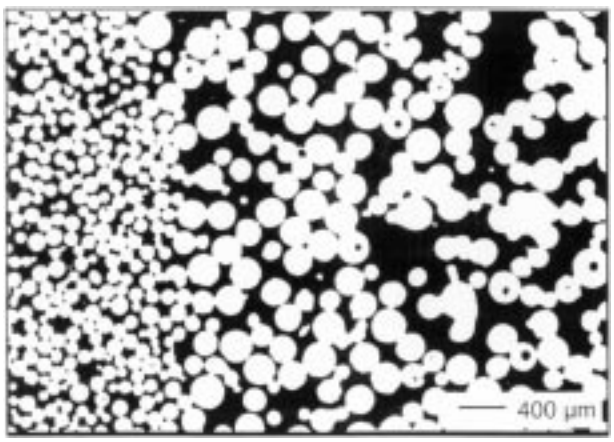

(a)

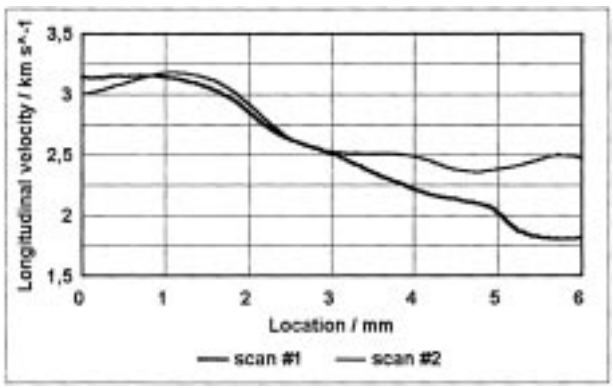

(b)

Figure 6 (a) Microstructure of a graded specimen (type #1, see text; cross-sectioned); (b) dependence of the longitudinal velocity on the location along the gradient as determined by PSAM.

Acknowledgment

The authors are indebted to Deutsche Forschungsgemeinschaft which supported these studies within the Schwerpunktprogramm Gradientenwerkstoffe under the contract numbers WI 1475/1 and GR 566/6. Further, the authors appreciate the careful metallographic work of Mrs B. Engelmann.

References

1. C. M. AGRAWAL, *JOM* **50** (1998) 31.
2. T. M. TURNER, D. R. SUMNER, R. M. URBAN, D. P. RIVERO and J. O. GALANTE, *J. Bone and Joint Surg.* **68–A** (1986) 1396.
3. U. ZWICKER, in ''Titan und Titanlegierungen'' (Springer, Berlin, 1974) p. 97.
4. H. J. BREME and J. A. HELSEN, in ''Metals as Biomaterials'', edited by J. A. Helsen and H. J. Breme (Wiley, Chichester, 1998), p. 25.
5. E. WINTERMANTEL and S.-W. HA, in ''Biokompatible Werkstoffe und Bauweisen'', (Springer, Berlin, 1996) p. 98ff.
6. D. T. REILLY, A. H. BURSTEIN and V. H. FRANKEL, *J. Biomech.* **7** (1974) 271.
7. J.-Y. RHO, *Ultrasonics* **34** (1996) 777.
8. J.-Y. RHO, M. E. ROY II, T. Y. TSUI and G. M. PHARR, *J. Biomed. Mater. Res.* **45** (1999) 48.
9. S. F. HULBERT, F. A. YOUNG, R. S. MATHEWS, J. J. KLAWITTER, C. D. TALBERT and F. H. STELLING, *J. Biomed. Mater. Res.* **4** (1970) 433.
10. J. D. BOBYN, R. M. PILLIAR, M. D. CAMERON and G. C. WEATHERLY, *Clin. Orthopaed. and Rel. Res.* **150** (1980) 263.
11. W. WINKLER-GNIEWEK, in ''Die Plasmapore-Beschichtung für die zementlose Verankerung von Gelenkendoprothesen'' (Aesculap, Tuttlingen, 1989) p. 6.
12. R. M. PILLIAR, *The Int. J. Powder Metallurgy* **34** (1998) no. 8, 33.
13. V. BIEHL, J. BREME, W. SCHULTE, B. D'HOEDT and K. DONATH, in Proceedings of the Werkstoffwoche '96, Symposium 4 ''Werkstoffe der Medizintechnik'', Stuttgart, May 1996, edited by J. Breme (DGM, Frankfurt, 1997) p. 177.
14. T. TARVAINEN, I. PARONEN, T. TUNTURI, J. RAUTAVUORI, P. TÖRMÄLÄ, H. PÄTIÄLÄ and P. ROKKANEN, *J. Mater. Sci.: Mater. Med.* **9** (1998) 509.
15. R. KUMAGAE, M. YOSHITAKE, K. HIDAKA and M. TOKIZANE, *J. Jpn. Soc. Powder and Powder Metallurgy* **42** (1995) 741.
16. D. J. KIM and W. GRILL, *Ultrasonics* **36** (1998) 233.
17. W. GRILL, K. HILLMANN, K. U. WÜRZ and J. WESNER, in ''Advances in Acoustic Microscopy'', Vol. 2, edited by A. Briggs (Plenum, New York, 1996).
18. R. W. RICE, *J. Mater. Sci.* **31** (1996) 1509.
19. A. S. HELLE, E. EASTERLING and M. F. ASHBY, *Acta metall.* **33** (1985) 2163.
20. T. B. MASSALSKI (editor), in ''Binary Alloys Phase Diagrams'', Vol. III (ASM Intl., Metals Park, 1990), p. 3371.
21. T. K. K. KHALIL, U. MÜLLER and G. ONDRACEK, *Mat.-wiss. u. Werkstofftech.* **27** (1996) 119; *ibid.* **27** (1996) 165; *ibid.* **27** (1996) 227.
22. T. KITSUGI, T. NAKAMURA, M. OKA, W.-Q. YAN, T. GOTO, T. SHIBUYA, T. KOKUBO and SH. MIYAJI, *J. Biomed. Mater, Res.* **32** (1996) 149.
23. S.-B. CHO, F. MIYAJI, T. KOKUBO, K. NAKANISHI, N. SOGA and T. NAKAMURA, *ibid.* **32** (1996) 375.
24. A. R. BOCCACCINI, G. ONDRACEK and E. MOMBELLO, *J. Mater. Sci. Lett.* **14** (1995) 534; A. R. BOCCACCINI, *ibid.* **16** (1997) 683.
25. M. ARNOLD, A. R. BOCCACCINI and G. ONDRACEK, *J. Mater. Sci.* **31** (1996) 1643.
26. W. KREHER, personal communication, 1997.
27. H. LEDBETTER, M. DUNN, S. KIM and R. FIELDS, in ''Review of Progress in Quantitative Nondestructive Evaluation'', Vol. 14, edited by D. O. Thompson and D. E. Chimenti (Plenum, New York, 1995) p. 1633; H. LEDBETTER, S. DUNN, M. DUNN, *ASME J. of Engineering Materials and Technology* **117** (1995) 402.
28. ANONYMOUS, in ''Porous Coating Report'' (Biomet, Warsaw, Indiana, 1986).

Received 4 May 1999
and accepted 24 January 2000